

promoting access to White Rose research papers



Universities of Leeds, Sheffield and York
<http://eprints.whiterose.ac.uk/>

This is an author produced version of a paper published in **Chemical Engineering Science**.

White Rose Research Online URL for this paper:
<http://eprints.whiterose.ac.uk/4063/>

Published paper

Dupont, V., Ross, A.B., Knight, E., Hanley, I. and Twigg, M.V. (2008)
Production of hydrogen by unmixed steam reforming of methane, Chemical Engineering Science, Volume 63 (11), 2966 -2979.

Production of hydrogen by unmixed steam reforming of methane

V. Dupont*, A. B. Ross, E. Knight, I. Hanley, M.V. Twigg^a

Energy and Resources Research Institute, University of Leeds, Leeds, LS2 9JT, UK

^a Johnson Matthey Plc, Orchard Road, Royston, SG8 5HE, UK

Unmixed steam reforming is an alternative method of catalytic steam reforming that uses separate air and fuel-steam feeds, producing a reformat high in H₂ content using a single reactor and a variety of fuels. It claims insensitivity to carbon formation and can operate autothermally. The high H₂ content is achieved by in-situ N₂ separation from the air using an oxygen transfer material (OTM), and by CO₂ capture using a solid sorbent. The OTM and CO₂ sorbent are regenerated during the fuel-steam feed and the air feed respectively within the same reactor. This paper describes the steps taken to choose a suitable CO₂-sorbent material for this process when using methane fuel with the help of micro reactor tests, and the study of the carbonation efficiency and regeneration ability of the materials tested. Elemental balances from bench scale experiments using the best OTM in the absence of the CO₂ sorbent allow identifying the sequence of the chemical reaction mechanism. The effect of reactor temperature between 600 and 800°C on the process outputs is investigated. Temperatures of 600°C and 800°C under the fuel-steam feed were each found to offer a different set of desirable outputs. Two stages during the fuel-steam feed were characterised by a different set of global reactions, an initial stage where the OTM is reduced directly by methane, and indirectly by hydrogen produced by methane thermal decomposition, in the second stage, steam reforming takes over once sufficient OTM has been reduced. The implications of these stages on the process desirable outputs such as efficiency of reactants conversion, reformat gas quality, and transient effects are discussed.

Keywords Hydrogen, methane, CO₂ sorbent, Oxygen transfer, reforming, carbon

* corresponding author

1. Introduction

Unmixed steam reforming, henceforth called ‘USR’, first appeared in the mainstream scientific literature through the two publications Kumar et al (1999) and Lyon and Cole (2000). It offers an alternative method for the autothermal production of a hydrogen-rich reformat (more than 90% dry). It relies on alternated feeds of air and of a mixture of vapourised fuel and steam to create a cyclic process. During USR, the fuel-steam feed and the air feed do not mix, contrary to conventional autothermal catalytic steam reforming, where pure oxygen is relied on for partial oxidation of the fuel and providing heat for the endothermic steam reforming reaction. Instead, the USR process makes use of an oxygen ‘mass transfer’ material or OTM, here chosen to be reduced nickel supported on alumina. Although various reactor and flow configurations are possible with USR, a plug flow fixed bed reactor is used in the present study, where the bed materials are crushed to 1-2 mm size. The OTM is able to store oxygen exothermically by forming the NiO oxide on the support when subjected to an air flow, thus heating up the reactor bed evenly over its cross-section, and allowing the inert N₂ component to evolve separately from the reformat. The oxide then regenerates to metallic Ni by reduction when it is exposed to the subsequent fuel and steam feed, responsible for the main steam reforming reaction. When a CO₂ sorbent material is used in combination with the OTM, the catalytic reaction of steam reforming proceeding under the fuel-steam feed on the hot Ni-OTM catalyst bed occurs alongside CO₂ capture. This results in further purification of the reformat as well as favouring the water gas shift reaction towards H₂ production. The reformat can reach more than 90% content in H₂ (dry) as a result of the combined in-situ N₂ and CO₂ separations and the increased WGS. Some of the heat liberated under the following air flow is then utilised to decompose the carbonate present, thereby regenerating the CO₂ sorbent for the next cycle while the Ni-OTM oxidises. The evolutions of CO, CO₂ and H₂ proceed under the fuel-steam feed. Under air feed, the reactor effluent is an oxygen-depleted and CO₂-laden air stream. When using one fixed bed reactor, the production of hydrogen is therefore intermittent. For the process to continuously produce hydrogen, two identical reactor beds would need to run in parallel, each operating in a different half cycle. Alternative ways of continuously producing H₂ with a single reactor could also involve the use of a rotating bed travelling through air feed then fuel-steam feed zones. Unmixed steam reforming has previously been demonstrated using methane and diesel fuels (Kumar et al, 1999, and Lyon and Cole, 2000). Over subsequent years, DOE reports and conference presentations appeared in the literature as research and development continued from the original work and the terminology of autothermal cyclic reforming (Kumar et al, 2004), as well as unmixed fuel processing were also used in this context (Zamansky, 2002, Rizeq et al,

2003,). Close relatives of unmixed steam reforming are chemical looping combustion (Ishida et al, 1987, Son et al, 2006), and coal hybrid combustion-gasification chemical looping (current work by the US' DOE National Energy Technology Laboratory).

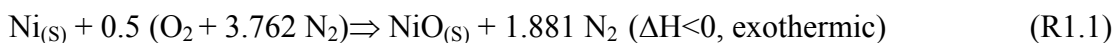
A number of advantages are claimed for the USR process: (i) production of H₂-rich reformat (ca. 90% dry H₂) with a single reactor, (ii) potential for autothermal operation without the need for pure oxygen that would require a costly air separator pre-processing stage, (iii) improved heat transfer characteristics that allow down-scaling up of the process to a point, increasing its potential for distributed power generation if coupled with an intermediate temperature solid oxide fuel cell, or with a molten carbonate fuel cell, (iv) low cost reactor materials due to a hotter reactor center and colder walls, (v) compactness of the process due to coupling of the endothermic and exothermic reactions within the reactor rather than relying on external heating, (vi) separation of CO₂-containing effluent from the H₂-rich reformat with potential for cheaper purification downstream technologies, (vii) insensitivity to coking, (viii) insensitivity to sulphur (as claimed by Lyon and Cole, 2000), finally, and related to the last two points, (ix) fuel feedstock-flexibility (gas and liquid). Currently there are adaptations of the principle of USR to pulverised coal using circulating fluidised beds technology which draw similarities with chemical looping combustion (Rizeq et al, 2003).

The cycle of reactions involved in the methane unmixed reforming process is shown below and includes some reactions that were identified during the present investigation in addition to those mentioned in the literature.

First half of cycle: air feed

The main reactions are

Oxidation of the supported OTM and separation of N₂ from air:



Reaction (R1.1) heats up the OTM's bed and some of its heat is used in the regeneration of the CO₂ sorbent:



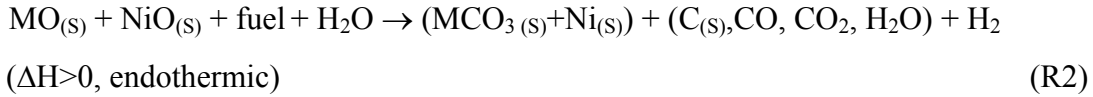
In addition to R1.1 and R1.2, identified in Lyon and Cole (2000) as the reactions at work under air flow, reactions R1.3 and R1.4 were found to play a significant role during the present work:



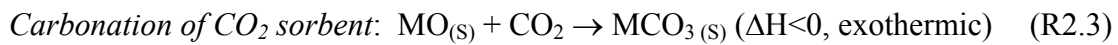
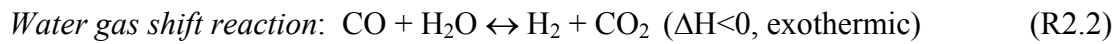
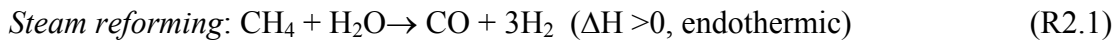
The gas product from this half cycle is a N₂ rich containing CO₂ and unreacted O₂.

Second half of cycle: fuel-steam feed

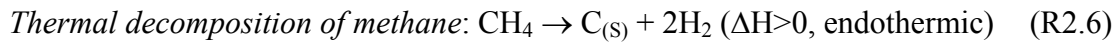
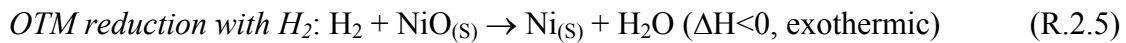
The vapourised fuel and steam mixture encounters the hot reactor bed and the following global reaction occurs:



Reaction (R2) is the overall reaction, it can be split up into the global reactions below:



OTM reduction with methane (unmixed combustion of methane)



The main mechanism of unmixed reforming is illustrated in figure 1.

Similar processes such as chemical looping combustion and sorption-enhanced gasification or reforming in circulated fluidised beds offer similarities of chemical mechanism to unmixed combustion, although these terms seem to have been so far applied to interconnected fluidised or circulating beds through which the OTM and/or the CO₂ sorbent circulate undergoing redox or absorption/desorption stages. Since the birth of chemical looping combustion (Richter and Knoche, 1983, Ishida et al, 1987), this technology has been the object of intense research worldwide due to its potential in clean combustion and combined heat and power (Son and Kim, 2006). Absorption enhanced gasification/reforming is used for syngas and H₂ production from coal (Lin et al, 2001) and biomass (Marquardt-Mollenstedt et al, 2004).

Figure 1 here

With carefully chosen feed flows and durations, as well as the right OTM to CO₂-sorbent ratio, Lyon and Cole (2000) demonstrated that the process could run autothermally, ie., without external heating and in a stable manner. When in autothermal operation, the reactor temperature oscillates during each cycle, with the lowest temperatures during fuel-steam feed and the highest at air feed, this in turn affects slightly the purity of the H₂ rich stream.

This paper describes firstly the methodology for the selection process of a suitable CO₂-sorbent, by focussing on (i) carbonation capacity/efficiency and (ii) regeneration capacity derived from TGA and micro-reactor tests. The second part contains results from bench scale

reactor experiments of unmixed steam reforming of methane under near isothermal conditions over a range of temperatures to determine the optimum conditions. Methane was chosen initially to study the reaction mechanisms of the process. Also, due to the lack of information on the unmixed steam reforming process in the literature to date, it was deemed necessary to investigate the chemical mechanism in detail under isothermal conditions, before autothermal operation could be attempted.

2. Experimental

CO₂ sorbent tests

The micro-reactor (plug-flow) was designed for the sole purpose of testing OTMs and CO₂ sorbents while a bench-scale reactor was being constructed to test the USR process. Although numerous OTM redox experiments were conducted in the microreactor, their outcome did not help identify a superior OTM, with all but one Ni-based commercial catalyst (Johnson Matthey) deemed suitable for the subsequent bench scale experiments. These experiments are reported elsewhere (Ross et al, 2003 & 2006). Overall, the OTMs showed a capacity to repeatedly oxidise under air flow and then subsequently reduce under both hydrogen and methane flow. Given the absence of steam in these experiments our conclusions were that we could test a smaller subset of OTMs at bench scale under unmixed steam reforming conditions, and the results for the most performant OTMs are reported here.

The experimental rig for the micro-reactor was built from narrow bore tubing (0.25 inch) and utilised a quartz silica reactor, fitted with a sintered platform for the support of OTM test material. All gas flows to the reactor were ensured by MKS mass flow controllers. The reactor temperature was measured by placing a K type thermocouple in the centre of the reactor and recording temperature readings using a PICO thermocouple logger. The following dry gas volume concentrations were monitored online using analysers from ABB: Uras 14 for CO, CO₂ and CH₄, Magnos 106 for O₂ and Caldos 15 for H₂. The gas reaching the analysers was dry and at room temperature. The resolution of the analyser stack was 0.1 vol %.

[Figure 2 here](#)

Thermogravimetric analysis (TGA) was also performed for all the CO₂-sorption materials tested to obtain their decomposition temperature. Carbonates of magnesium, calcium, barium and strontium were investigated by TGA using the temperature profile of 25°C heating to 1400°C using 20°C min⁻¹ in a nitrogen atmosphere. In each case the decomposition temperature was measured.

Adsorption testing of the CO₂ sorbents (reaction R2.3) was performed in the plug flow reactor described in Figure 2. A sample of sorbent (1g) was placed into the reactor and heated to 800°C under a continuous nitrogen flow (50 sccm) to pre-calcine the material and allow regeneration of the material. The reactor was cooled to 700°C whereby the flow was switched to CO₂ (21.5 sccm) for a period of 10 min, following which the reactor was cooled to laboratory temperature. The flow was then switched to nitrogen (54 ml min⁻¹) and the reactor heated at 20°C/min to 800°C and held for 10 minutes, during which time the evolved CO₂ was measured by on-line analysers. Total CO₂ liberated was used as a measure of sorbent capacity.

For successful materials, adsorption/desorption reactions were cycled to evaluate regeneration capacity and stability. They were first regenerated at 800°C for 15 min, the reactor was cooled to 700°C and the flow switched to CO₂ for 10 min. This procedure was repeated through ten cycles.

Bench scale experiments of unmixed reforming of methane on fixed bed reactor

A diagram of the bench scale experimental set up is given in Fig.3. The reactor had an internal volume of 80 cm³. It contained in the first tests reported here, 80 g of a Ni-based OTM (27.5 wt.%). In the final experiment, a bed consisting of a mixture of 60 g of the OTM and 20 g of the calcined dolomite selected from the micro-reactor tests was used. The bed material was in ground pellets form of approximately 1-2 mm size, and enclosed by two plugs of inert alumina particles. In the present study, the reactor was heated externally by a 1 kW coiled tubing heater. The heating element was first clad with K wool then surrounded by an alumina casing, itself enclosed in a stainless steel casing. Isothermal conditions under the endothermic stages of fuel-steam feed and nitrogen flow were maintained by heating the main reactor to 600- 800°C with the external heating coil in on-off feedback loop control, using the mid-reactor thermocouple temperature as the output variable. Under the exothermic conditions of the reactor under the air flow feed, the reactor was left to undergo the natural exotherms without external cooling and still under the on-off heating control. At start up, once the reactor temperature had been achieved, the fuel feed step was commenced.

The feed gas flows were maintained by three mass flow controllers (MKS), one each for nitrogen, methane and air followed by three solenoid valves operated centrally in sequence using the pulse sequence generator. The liquid feed of water was regulated by a peristaltic pump followed by another three way valve controlled by the pulse sequence generator. When the unit was not operating (not cycling), a third valve allowed flushing of the assembly with

nitrogen gas. The product gases were cooled using a water-cooled condenser before entering a water trap (ice bath), followed by a chemical water trap (silica gel). The dry gaseous products were fed through a series of analysers, the same as those described in the microreactor tests. The following gas volume concentrations were monitored on-line and data-logged: CO, CO₂, CH₄, H₂ and O₂, using the ABB analysers.

The gas reaching the analysers was dry and at room temperature. For safety reasons, the entire gas product stream was diluted with air as well as additional N₂, and disposed of by flowing it through a catalytic burner (enclosed heated platinum gauze). Two relief valves were situated before and after the reactor to maintain the reactor pressure below 2 bar. Pressure readings (inlet and outlet) and temperature (lower, middle and upper reactor) were monitored at the points in the rig shown in Fig. 3. The three thermocouples were located so that the lower position and the upper position were still embedded in the OTM bed. The calculations of conversion efficiency of methane, water, and NiO, as well the rates of carbon formation rates and NiO reduction are provided in the appendix.

[Figure 3 here](#)

3. Results and discussion

Results from the micro-reactor tests of CO₂ sorbents:

A number of sorbents were identified for evaluation. Methods for testing CO₂ adsorption were developed. The sorbents were categorised into two main groups (i) minerals (dolomite, calcite, magnesite and limestone), and (ii) modified supports (CaCO₃ from acetate, CaCO₃ on γ -Al₂O₃, Mg-hydrotalcite, Ca-hydrotalcite and blank γ -Al₂O₃). Initial TGA experiments of Ba, Sr, Ca and Mg carbonates thermal decomposition indicated that Mg and Ca based sorbents would be suitable within the reaction temperature range having a decomposition temperature of 550 °C and 806 °C under nitrogen atmosphere respectively.

Table 1 lists the theoretical (from maximum CO₂ content) and the experimental CO₂ adsorption capacity for each of the materials in g of CO₂ per kg of sorbent. The experimental capacity was measured as described in the experimental from the CO₂ evolved during calcination under N₂ flow, following carbonation at 700 °C in pure CO₂ flow. For some minerals, several sources were tested and the maximum values were reported. For impregnated materials, calcinations were performed with a relatively fast heating rate in nitrogen (5 °C/sec).

[Table 1 here](#)

Preparation of sorbents by calcination of calcium acetate and mineral calcite exhibited the highest experimental adsorption of CO₂ /kg sorbent, followed by dolomite and limestone. However calcined dolomite makes best use of its theoretical capacity for CO₂ adsorption (63.5%) under the conditions tested. Ca and Mg hydrotalcite supports performed poorly, as expected given the severe temperatures of carbonation and calcinations used here. This is due to first, loss of their H₂O interlayer up to 200°C, followed by the irreversible dehydroxylation and decarbonisation above 500°C, leaving a spinel structure (Reijers et al, 2006). Similarly, magnesite was also used outside of its optimal carbonation-calcination range, yielding a poor 3.9% capacity for CO₂ adsorption used during the test. All carbonation tests were performed at 700°C, which was initially the proposed operating temperature of the bed during the fuel/steam step. Carbonation was very sensitive to temperature. For calcium oxide, CO₂ chemisorption increased with temperature below 700°C and decreased with temperature above 700°C in 100% CO₂, in agreement with the thermodynamics of the material. The choice of sorbent is highly dependent on the operating temperature of the reactor for both steps of the unmixed reforming cycle.

Previously a 1:4 ratio of Ni to Ca was used to attain autothermal behaviour for methane unmixed reforming (Lyon and Cole, 2000), using calcined dolomite as the sorbent material. Carbonation capacities after repeated cycles of the three best sorbents, calcite, dolomite and CaCO₃ (from Ca acetate) are shown in Figure 4 for a stoichiometric flow of CO₂. Carbonation capacity following initial calcination and regeneration creates surface area growth resulting in high chemisorption capacity. This decreased upon further cycling due to a combination of pore blocking and sintering, however, the surface area available for carbonation was expected to fall over time (Agnew et al, 2000). Further studies are still required to investigate the dependence of diffusion and pore size distribution. After a steady state had been achieved, the results indicated the CaO/CaCO₃ prepared from calcium acetate exhibited a similar sorption capacity to the calcined dolomite. The mineral dolomite investigated here had the following composition by weight of 29.4% CaO, 19.3% MgO, 3.8% SiO₂, 1.7% Al₂O₃, 0.6% Fe₂O₃, < 0.1% K₂O, with balance CO₂, and originated from Spain (Sierra de Arcos). The same material has been used for H₂S removal by Agnew et al (2000) and Adanez et al (1998). We show in Dupont et al (2007) that this dolomite behaved very similarly to other dolomitic rocks during thermal decomposition and carbonation cycles in CO₂ atmosphere under the same heating and cooling rates of TGA cycles as those reported in Chrissafis et al (2005). To summarise, the experiments showed that after the first thermal decomposition, the MgO compound of the dolomite was unable to re-carbonate, whereas CaO could be repeatedly re-carbonated. Under

1 atm partial pressure of CO₂ of the TGA experiments in pure CO₂ atmosphere, the thermal decomposition of the CaCO₃ occurred between 920°C and 940°C, whereas subsequent carbonation upon cooling began below 860°C. Figure 5 shows the mass % of the Spanish dolomite during three calcinations upon heating alternated with two carbonation upon cooling in TGA runs at 1 atm under flows of (i) 100% CO₂, (ii) 50% CO₂-50% N₂, and (iii) 100% N₂ (one calcination run only).

[Figure 5 here](#)

The top row of Table 1 indicates that the theoretical mass gain for this dolomite as a result of full carbonation is 23.9 wt% (238.6 g CO₂/kg sorbent). It is therefore possible to compare the experimental CO₂ mass gain from carbonation for the 100% CO₂ and the 50% CO₂ flows with the theoretical value. The CO₂ intake can be derived from the mass % difference between the middle horizontal plateau and the lowest horizontal plateau of Fig. 5. For 100% CO₂ flow, the difference was 13% (from 59% to 72%), equivalent to 54% of the theoretical capacity having been used. With a 50% CO₂ flow, it was 16 wt% (from 57-76%), i.e. 67% of the theoretical capacity. This result was counterintuitive and could be explained by the sample's history during the previous thermal decomposition in the same atmospheres. Indeed, with the 100% complete decomposition had not occurred, with a final mass 59% as opposed to 57% for 50% CO₂ atmosphere, leaving a lower capacity for the following carbonation. Clearly there is a dependence of the sorbent capacity used on the partial pressure of CO₂, and for this material, using 100% of its sorption capacity has not been realised. It is possible that carrying out the TGA runs up to 1100°C would have caused sintering to the material, accounting for these poor capacities used. Figure 5 also shows that the temperature at which calcinations began upon heating decreased significantly with decreasing partial pressure of CO₂ in the flow. This would be expected as the imposed presence of CO₂ during calcination would hamper the removal of the CO₂ product from the material via diffusion, in addition, it could also favour residual carbonation. The USR process expects the calcination of the sorbent to occur under air feed, but if for instance significant carbon had deposited during the previous fuel and steam feed, its combustion during the air feed would raise the partial pressure of CO₂, therefore also raising the temperature required for the sorbent regeneration. This could be addressed by the added exothermicity of the carbon combustion, but it is not known whether that would be sufficient. At any rate, the increased temperature of calcination would have detrimental effects on the sorbent's stability as well as the OTM's. There is therefore a strong

incentive to minimise carbon formation during the fuel-steam feed, regardless of potential deactivation caused to the OTM by coking.

From the point of view of carbonation, increasing the partial pressure of CO₂ also seemed to increase the temperature where carbonation began upon cooling (820°C for 50% CO₂ compared to 870°C for 100% CO₂). In the USR process, the CO₂ content varies is typically around 10% in absence of N₂ diluent, whereas this would be beneficial by lowering the temperature ranges of both carbonation and calcination, and therefore increase the thermal efficiency of the process while offering better conditions for the materials stability, it remains to be determined whether the capacity would be adversely or positively affected for the lower CO₂ partial pressures. The literature on the effect of CO₂ partial pressure on CO₂ sorbents experimental intake indicates that capacity can decrease significantly for CO₂ partial pressures below 0.5 bar and even further under the combined effects of repeated cycling and steam contents above 20% (Ochoa-Fernandez, 2007). The USR conditions for sorbent carbonation under fuel-steam feed and reactor pressure at 1 bar would combine low CO₂ partial pressures (ca. 0.1 bar), high steam content (between 0.2 and 0.9 bar), and would require frequent cycling (every 6-10 min). Being able to maintain the high H₂ purity flow which requires a stable, high capacity, water insensitive CO₂ sorbent will therefore be a very significant challenge for the USR process. This challenge is shared by all processes of sorption enhanced steam reforming.

Results from the bench scale unmixed steam reforming isothermal tests

Figure 6 shows the reformat composition when operating a fuel-steam feed at a steam to carbon ratio of 4, a temperature of 650°C, with a bed material consisting in 20 g of calcined dolomite and 60 g of OTM (27.5 wt% Ni catalyst from JM)). These runs are performed without nitrogen diluent. The amount of dry hydrogen production is strongly influenced by temperature mainly due to the performance of the CO₂ sorbent. The dolomite CO₂-sorbent used in these studies has already been through four cycles, by which time the extent of deactivation due to pore blocking etc had reached a relatively constant level (see Fig. 4). During the USR process the CaCO₃ is regenerated in air, the temperature required to completely decompose this particular dolomite in air was 780°C. Operation of the reactor at lower temperatures e.g. 600°C resulted in a smaller temperature swing during the oxidation cycles (peak at 750°C), short of both the decomposition temperature of CaCO₃ in nitrogen and in air. Regeneration could not have taken place for this run. Operation of the reactor at higher

temperatures (eg 700°C) resulted in a higher temperature swing (peak at 1020°C) well above the decomposition temperature of dolomite in both air and N₂, therefore regeneration was possible. However a reactor maintained at 700°C would have resulted in a lower conversion during carbonation. These results were included here to demonstrate the potential of USR for producing a high purity H₂ reformat.

[Figure 6 here](#)

The remainder of the experiments presented in this paper were performed in absence of CO₂ sorbent and with a steam to carbon ratio (S:C) of 1.8. In previous work (Dupont et al, 2007), we analysed the effects that the nature and amount of OTM, as well as the flow of methane, had on the process outputs for the near isothermal conditions of 800°C. Results using sunflower oil as the fuel were also presented. In the present work, the effects of reactor temperature from 600°C to 800°C on the process outputs when using methane as the fuel and in the absence of CO₂ sorbent are reported. The duration of the feed flows were chosen to be sufficiently long to achieve a steady state whenever possible, this was achieved in 10 minutes of constant feed flow. Most of the outputs were derived from elemental balances using the online monitoring of the dry O₂, CO, CO₂, CH₄ and H₂ content in the reformat, the molar flow feeds (CH₄, air, N₂, and water), and from the knowledge of the amount of Ni in the OTM. Although carbon deposition does not always involve pure carbon, but carbon rich sooty deposits, for the sake of simplicity we considered the species C_(s), CO and CO₂ as the only carbon-containing products in these balances. The absence of higher carbon species in the gas phase was verified sporadically by off-line GC-FID analyses.

In the section below, we show how manipulating the N, C, H and O balances can yield the conversions of water, fuel and Ni/NiO, as well as rates of NiO reduction/oxidation, carbon formation/removal, and total carbon formed or removed over the duration of the full fuel/steam feed and air feed. Since these calculations rely on the assumed simultaneous measurements of the dry online gas analysers, we then present a discussion on the effects that the analysers speed of response for the various species could have had on the conversions and rates calculations, as well as the effects that differences in retention of the various species by the loaded reactor and silica gel trap might have had.

Theory of the calculation of conversions and rates from elemental balances:

Two types of balances have been carried out, one based on a CH₄/N₂/steam feed, the other based on air feed. The same nomenclature is used throughout and the theory set out in Eqs. 1-15.

The sampling time interval is dt , the total molar flow rates and the molar flow rate of species i at time t are \dot{n} and \dot{n}_i respectively. The subscripts ‘dry’, ‘in’ and ‘out’ refer to conditions following water removal, and at reactor inlet and outlet respectively. The change in moles of i present in the reactor during dt is dn_i , this value is positive when i accumulates in the reactor. The dry mol fractions measured by online analyses are x_{CH_4} , x_{CO} , x_{CO_2} , x_{O_2} , x_{H_2} . The mol fraction of N_2 (x_{N_2}) is not measured but is derived from

$$x_{N_2} = 1 - (x_{CH_4} + x_{CO} + x_{CO_2} + x_{O_2} + x_{H_2}) \quad (1)$$

$$\text{The } N_2 \text{ balance then yields: } \dot{n}_{out,dry} = \frac{\dot{n}_{N_2,in}}{x_{N_2}} \quad (2)$$

(a) Elemental balance calculations of the CH_4/N_2 /steam feed:

The hydrogen balance on 2H basis yields

$$\dot{n}_{H_2O,out} = (2\dot{n}_{CH_4,in} + \dot{n}_{H_2O,in}) - \dot{n}_{out,dry}(2x_{CH_4} + x_{H_2}) \quad (3)$$

and the water conversion efficiency is then given by

$$H_2O_{conv}(\%) = 100 \times \frac{(\dot{n}_{H_2O,in} - \dot{n}_{H_2O,out})}{\dot{n}_{H_2O,in}} \quad (4)$$

When H_2O_{conv} is negative, there is a net production of water, when positive there is a net consumption of water.

$$\text{The } CH_4 \text{ conversion efficiency is } CH_4_{conv}(\%) = 100 \times \frac{(\dot{n}_{CH_4,in} - x_{CH_4} \times \dot{n}_{out,dry})}{\dot{n}_{CH_4,in}} \quad (5)$$

In the absence of CO_2 sorbent, the carbon balance is

$$\frac{dn_C}{dt} = \dot{n}_{CH_4,in} - \dot{n}_{out,dry} \times (x_{CH_4} + x_{CO} + x_{CO_2}) \quad (6) \text{ and } n_C = \int_0^t \frac{dn_C}{dt} \times dt \quad (7)$$

Where dn_C/dt is molar rate of carbon formation and n_C the moles of carbon present in the reactor at a given time t .

Also in the absence of CO_2 sorbent, the oxygen balance is given by:

$$\frac{-dn_O}{dt} = ((\dot{n}_{H_2O,in} - \dot{n}_{H_2O,out}) - \dot{n}_{out,dry}(x_{CO} + 2x_{CO_2} + 2x_{O_2})) = \frac{dn_{NiOred}}{dt} \quad (8)$$

Where $-dn_O$ is the molar amount of oxygen depleted from the reactor during dt (by reduction of NiO to Ni). dn_{NiOred}/dt is the molar rate of NiO reduction.

$$\text{The conversion of NiO to Ni at any time } t \text{ is } NiO_{conv}(\%) = 100 \times \frac{n_{NiOred}}{n_{NiO}} \quad (9)$$

$$\text{where } n_{NiOred} = \int_0^t \frac{dn_{NiOred}}{dt} \times dt \quad (10)$$

and n_{NiO} is the molar amount of nickel present at $t = 0$.

(b) Elemental balance calculations of the air feed:

No H_2 or CH_4 were found to evolve from the reactor.

$$\text{The carbon balance yields: } \frac{dn_C}{dt} = \dot{n}_{out,dry} \times (x_{CO} + x_{CO_2}) \quad (11)$$

where dn_C is the molar amount of carbon consumed by oxidation reactions in interval dt .

$$\text{Molar amount of carbon consumed at } t \text{ is } n_{C,prod} = \int_0^t dn_C \quad (12)$$

$$\text{The oxygen balance yields: } \frac{dn_O}{dt} = 2\dot{n}_{O_2,in} - \dot{n}_{out,dry} \times (2x_{O_2} + x_{CO} + 2x_{CO_2}) \quad (13)$$

$$\text{The conversion efficiency of Ni to NiO is } Ni_{conv}(\%) = 100 \times \frac{n_O}{n_{Ni}} \quad (14)$$

$$\text{where the molar amount of oxygen reacted is } n_O = \int_0^t \frac{dn_O}{dt} \times dt \quad (15)$$

c) Elemental balance calculations of the N_2 feed

A N_2 only feed is used after the fuel/steam feed to purge its products and separate them from those of the following air feed. Accounting for the products evolving during the N_2 feed is important when carrying out the carbon formation/removal and Ni/NiO balances over a whole cycle. The equations for this step are the same as those of the air feed where $\dot{n}_{O_2,in}$ is set to zero.

Effects of species retention in the reactor, silica gel trap and analysers

Experiments using two calibration gases (25% CH_4 , 20% CO , 25% CO_2 , balance N_2) and (80% H_2 , balance N_2) respectively, were performed to assess the retention times of the various elements in the path of the analysis. Firstly, these gases was flowed through the analysers with and without the silica gel trap present upstream of the analysers. The response times were measured, represented by t_{0+} and t_{90} , i.e. the time where the gas species is first detected from the time of flow start (species breakthrough), and the time at which 90% of the calibration value is reached, respectively. Values of t_{0+} and of $t_{90} - t_{0+}$ are shown in Table 2.

[Table 2 here](#)

It can be seen that the t_{0+} of CH_4 , CO_2 and CO are the same (15 s) in the absence of silica gel trap, with H_2 breakthrough delayed by 5 s, and when a silica gel trap is present, only CO breakthrough is delayed by an additional 5 s. The $t_{90} - t_{0+}$ indicate that CO is the fastest in reaching the calibration value, and CO_2 the slowest, with 7 s between them in the presence of

silica gel trap. Therefore the adsorption due to the silica gel was small. The next experiments were aimed at determining the retention introduced by physical interactions with the reactor bed in the presence of the silica gel trap. Firstly, a calibration gas was flowed over a reduced catalyst bed, and secondly over an oxidised catalyst bed, with and without steam present. The latter experiments were performed over a temperature range from 300°C to 800°C. At room temperature chromatographic retention was observed for all species particularly CO₂. As the temperature increased this retention was reduced, as would be expected from the increase of the resulting space velocity. However there was still a significant time lag for CO₂ at 400°C attributed to adsorption /desorption. At 400°C, it is possible to flow all four calibration gases through the loaded reactor without appreciable reaction. The t_{0+} and $t_{90} - t_{0+}$ measured for these experiments are shown in Table 3.

[Table 3 here](#)

The values of t_{0+} for the different species are most relevant when establishing the sequence of initial reactions, whereas the $t_{90} - t_{0+}$ measurements are relevant to the accuracy of selectivity of carbon gases at a given time. It was determined that when flowing calibration gas over an oxidised catalyst at 700°C, there was a 5 s delay between the detection of methane and that of CO₂, recorded at 35 s and 40 s respectively. During a CH₄/N₂/steam feed run at the same temperatures, we observed the same delay between the CH₄ and CO₂ breakthroughs, this bears on our discussion of the initial reactions sequence.

Results under CH₄/N₂/steam(fuel) feed and discussion

The flow of CH₄ was 358 sccm (i.e. 2.66×10^{-4} mol s⁻¹), water was 0.52 ml min⁻¹, yielding a steam to carbon ratio of 1.8. For all experiments, the CH₄, N₂ and steam were fed for a total of 600 s following which there was a further 200 s with N₂ flow only before switching to the air feed. The reactor pressure was between 1 and 2 atm. A nitrogen flow of 600 sccm was used as inert diluent allowing closure of the elemental balances. Results for reactor set temperatures of 600°C, 650°C, 700°C, 750°C and 800°C are reported in Table 4 and Figs 7-9. Firstly, the chemical mechanism during fuel-steam feed is discussed, secondly the effect of reactor temperature on the process outputs is considered.

(i) Reaction mechanisms during the CH₄/N₂/steam (fuel) feed step:

The sequence of events was characterised by the same type of observations for all the isothermal conditions tested. The dry gas composition (raw data) for the first 200 s of this feed at 750°C is shown in Fig. 7. It can be seen that in the initial 40 seconds no gas species

evolved from the reactor, at the end of there is CH₄ breakthrough. This can be attributed to the retention time of CH₄ by the combined effects of physical interactions with the reactor bed, silica gel trap and analyser response time. Then, CO₂, CO and H₂ breakthroughs followed in sequence. Since the bed is oxidised and there is steam in this initial stages, the t_{0+} values of Table 3 indicate that in the absence of chemical reactions, CH₄ breakthrough is expected first, followed 5 s later by H₂, and CO₂ and CO together. When attempting to identify the sequence of chemical reactions by subtracting the various species physical retention times, we can estimate that CH₄ and CO₂ are likely to have evolved first and simultaneously followed by CO and then H₂ also close to each other. The outputs from the elemental balance are illustrated in Figs.8-10, and are commented below in two stages.

Figures 8,9,10 here

The analytical information derived from the elemental balance is shown from the starting time of 40 s, before which the calculations were erroneously predicting 100% fuel conversion and 100% C_(s) selectivity, due pre-breakthrough conditions of the carbon containing gas species. Stage 1. In the initial period of the fuel feed (from 40 to 100 s), a very high conversion of methane was observed (98%) as illustrated in Fig. 8. Steam conversion showed a large negative value indicating water was not initially used as a reactant, and was instead produced in the reactor. The OTM reduction began with a sharp increase (Fig. 10). The selectivity of CO₂ from the carbon containing products (CO/CO₂/CH₄/C(s)) increased sharply from 5 % to 50% at 70 s (Fig. 9). The selectivity to C(s) was initially predicted to be high (95%) which then reduced to approximately 1.5%, however, it was probably artificially high due to the combined effects of physical interaction with the reactor bed and the response time of the analyser causing differences in the $t_{90} - t_{0+}$ between CH₄ and CO₂. In terms of reaction sequence, it is likely that of the methane converted, some was used by R2.4 (reduction of NiO-OTM by CH₄) producing CO₂ and water, and some was converted by thermal decomposition via reaction R2.6. Ni/Al₂O₃ is a well known catalyst of CH₄ thermal decomposition, but so are Ni/NiO catalysts. Couttenye et al (2005) found an increase of activity with increasing size of NiO crystallites. In addition carbons are also active in CH₄ thermal decomposition (Muradov et al, 2005). Given the absence of H₂ in the reactor effluent despite its short retention time, any hydrogen produced via thermal decomposition was therefore assumed to be entirely consumed by the OTM reduction reaction (R2.5), also creating water as a co-product. This mechanism explains the large initial negative H₂O

conversion of Fig. 8. The relative roles of the two CH₄ consumption reactions is somewhat skewed by the different retention times of CH₄ and CO₂, but would indicate that by the end of stage 1, reaction R2.4 dominates over R2.6. This is supported by the low selectivity of C_(S) and the increasing reduction rate of NiO. Throughout stage 1, the net steam conversion remained more or less constant and largely negative (Fig. 8). We conclude at this stage steam reforming was still dormant.

Stage 2: from 100 s until the end of the feed period (600 s), the net conversion of steam rose sharply, eventually raising above zero, and finally reaching a plateau at 52% (Fig.8). During this stage, the OTM reduction rate decreased equally sharply to near zero, while the CO₂ selectivity dropped as well to its minimum value, and the amount of H₂ in the reformat stabilised at around 76% (dry) (Fig. 9). This was concurrent with the selectivity of C_(S) plateauing at its lowest value ca. 4%. The interpretation of these events was that, in this final and principal stage, steam reforming (R2.1) first competed for fuel with NiO-OTM reduction by CH₄ (R2.4), and subsequently became dominant. The water gas shift reaction and its reverse (R2.2) reached equilibrium.

[Table 4 here](#)

(ii) Effect of temperature on process output performance

Table 4 shows a number of process outputs under CH₄/N₂/steam feed for temperatures ranging from 600°C to 800°C, including repeat runs. The tabulated values are an average of those obtained at the end of stage 2. Considering the closeness of the repeat experiments, a good accuracy is inferred from the experiments. A column headed ‘dead time’ in Table 2 represents the time of H₂ breakthrough in these reactive conditions.

In terms of desirable outputs of the fuel-steam feed runs, the ‘dead time’ should be as small as possible. In the conventional steam reforming process, water conversion is not closely monitored and is rarely reported in the literature because the process needs to operate with a large excess of steam (ca. 3) to use more favourable thermodynamic equilibrium of the water gas shift reaction while avoiding carbon accumulation by steam gasification. In theory, the USR process does not have the constraint of operating with such excess water. As a result, water conversion is an output parameter which, when maximised, could increase H₂ yield while producing a higher partial pressure of CO₂, i.e., better conditions with regards to a CO₂-sorber’s stability under repeated cycling. The latter is best illustrated by the CO/CO₂ ratio, which should be as small as possible to offer optimal carbonation conditions. An additional efficiency parameter was calculated in the form of H₂ production efficiency through the ratio

of molar outflow of H₂ to molar inflow of 2H from the combined CH₄ and H₂O feeds ('Prod Eff H₂' in Table 4). Finally, maximising the dry H₂ content in the reformat can save on the complexity of downstream H₂ purification stages, this value is headed 'dry (0N₂) H₂' because it is corrected for zero N₂ content in the reformat.

From Table 4, it is obvious that 600°C yielded poor results overall, with low methane conversion (around 50%), the lowest water conversion of the set (around 41%), these resulted in the lowest dry H₂ content in the reformat and lowest H₂ production efficiency. Only the 'dead time' and the CO/CO₂ ratio were the best of the set. In contrast, the tests at 800°C showed the highest methane conversions (99%), highest dry H₂ (75.2%) and highest H₂ production efficiency (~75%). Unfortunately, the 800°C tests also exhibited the longest dead time (80-100 s, i.e. 1/6 of the run duration) and worst CO/CO₂ ratio (~3). Considering the parameter outputs of Table 4 for the other temperatures, it was not possible to reach all the desirable goals simultaneously under the current process constraints.

The ratio of CO to CO₂ selectivity (last column in Table 4) was seen to increase with increasing reactor temperature, with 600°C yielding a ratio of 0.74-0.8, and 800°C a ratio near 3. These were compared against thermodynamics equilibrium predictions for steam methane reforming at steam to carbon ratio of 1.8, and pressures at 1 atm. Two types of calculations were performed, one in which graphitic carbon was not allowed to form, and another where it is present. The thermodynamic properties of graphitic carbon are well known which is why they were chosen here for discussion purposes. In contrast, those of the carbon deposits formed on catalysts are not readily available even though they would be best suited to this type of modelling. The results in absence of graphitic carbon exceeded the experimental CO/CO₂ ratios at best by 24% and at worst 58%. The model with graphitic carbon was deemed unsuitable as it overpredicted by an order of magnitude the carbon selectivity. This exercise highlights the need to include accurate thermodynamic properties for solid carbon formation from catalytic coking conditions.

The USR process is meant to operate in the presence of a CO₂ sorbent, thus the ratio of CO/CO₂ near 1 obtained between 600°C and 650°C indicated a better potential for carbonation in the presence of a CO₂-sorbent, compared to the poor ratio of 3 at 800°C. More importantly, the temperatures between 600°C and 650°C offer safer conditions for carbonation, as they are well away from the dolomite calcination temperature.

In previous work (Dupont et al, 2007), which compared the performance of different OTMs at the temperature of 800°C on 40 g of OTM bed material, it was shown how increasing the

methane flow from 152 sccm to 400 sccm at a steam to carbon ratio of 1.8 decreased the dead time dramatically from 200 s to 100 s for the same catalyst as the one used here. This was accompanied by a penalty on water conversion, with a drop from 47% to 38%. The implications of the presence of a 'dead time' will be crucial when autothermal conditions will be attempted. This is because the duration of the fuel-steam feed will be determined by how quickly the reactor bed material cools. It is reported that 5-6 minutes feed durations were ideal in powering a 20 kW fuel cell (Lyon and Cole, 2000). This is comparable to the 10 min of the CH₄/N₂/steam feed chosen here. Dead times of 100 s, i.e. 1/6 of the feed duration would therefore decrease considerably the overall process conversion efficiency (as opposed to its average over stage 2), as shown in Dupont et al (2007). Therefore a process modification aimed at eliminating dead time should be considered. Introducing a short fuel-only burst before the steam feed begins could considerably reduce the dead time by generating H₂ via thermal decomposition (R2.6) in excess of the NiO-OTM reduction rate demand, and also start the NiO reduction by methane (R2.4). This would ensure that NiO reduces quickly, and that H₂ exits the reactor at all times of both the fuel-only feed and the fuel-steam feed. The cost of steam recycling would be reduced and steam would not act as a heat sink, thereby improving reactant economy and overall energy efficiency of the process. As the NiO-OTM reduction would proceed faster, the steam reforming under the subsequent fuel-steam feed would start from the beginning of the feed, and would no longer compete with both R2.4 and R2.6 for fuel.

Results under air feed and discussion

The air feed, which represents half of the cyclic process under normal operating conditions, fulfils three important roles. When there is no CO₂ sorbent, air oxidises the Ni-OTM thereby heating up the bed, and thus an in-situ separation of the N₂ occurs. If there was any carbon left from the previous fuel-steam feed, it burns it off. In addition, when a CO₂ sorbent is present (not the case here), under the high temperature achieved by the OTM oxidation, the sorbent undergoes calcination, releasing the CO₂ captured during the previous fuel-steam feed and thereby regenerates. Given the exothermicity of the two reactions of carbon and Ni oxidation in the absence of CO₂ sorbent, the isothermal conditions previously observed under fuel-steam feed were no longer maintained. This is shown in Fig. 10 where the peak temperatures at three locations in the reactor (top, middle and bottom) following the fuel-steam feed at 750°C are plotted. A flow of 2000 sccm of undiluted air was used in this feed, corresponding to 3.125×10^{-4} mol s⁻¹ of O₂, and the duration of 250 s was chosen after realising that beyond

this time no reactions occurred. Figure 10 illustrates the exothermic swing in temperature during the oxidation step and shows that the temperature could reach over 1000°C from the initial set temperature of 750°C. During the fuel step, the temperature is controlled by external heating.

[Figure 10 here](#)

Figure 11 plots the O₂ conversion, Ni-OTM oxidation rate and Ni-OTM overall conversion calculated from the elemental balances, and begins at 30 s, the retention time for this feed. During the first 150 s of the air feed, the O₂ conversion of 100% and the plateaued OTM oxidation rate indicated that the Ni oxidation rate was limited by the O₂ feed. It then dropped suddenly beyond the 20% OTM conversion point to reach a near zero rate while O₂ conversion decreased to a very small value, possibly zero considering experimental errors. There are similarities in the rates of conversion of the OTM achieved via reduction under the fuel-steam flow and via oxidation under air flow.

[Figure 11 here](#)

Carbon and Ni/NiO balances over the whole cycle

Table 5 lists the %conversion of NiO to Ni during the two first feeds (CH₄/N₂/steam and N₂ feed) and the % conversion of Ni to NiO during the following air feed for the five temperature studied and their repeat experiment. The conversions of NiO to Ni and of Ni to NiO are remarkably close to each other to the exception of one run at 650°C (discrepancy between 11.5% and 19.6%). There is a clear trend of increase in conversion with increase in temperature, indicating that faster rates of reduction and oxidation were at work in the kinetic control regimes (early stages prior to the CH₄ and air feed rates controlling the rates of NiO reduction and Ni oxidation respectively). This will have consequences on future attempts to achieve autothermal behaviour, as the runs with little cyclic Ni/NiO conversion will exhibit the smallest exotherms and present a larger mass of material acting as a heat sink instead of fulfilling its reactive potential.

A similar full cycle balance is shown in Table 5 for carbon produced during the CH₄/N₂/steam and carbon oxidised during the N₂ and air feeds. Again, the total carbon produced was overall very close to the carbon oxidised over a full cycle. The largest discrepancies were found only for two runs, at 700°C, with 11×10^{-3} mol produced and 6.55×10^{-3} mol oxidised, and at 750°C, with 12×10^{-3} mol produced and 7.9×10^{-3} mol oxidised. The surprise was the realisation that during a N₂ feed following a CH₄/N₂/steam feed, a significant CO₂ evolution persisted, well in excess of the natural purge from the previous feed, unlike CO and H₂ which

decreased quicker in this feed. This indicated that the steam gasification of carbon with leftover steam was not the likely source of carbon removal, as it would have created CO and H₂, but instead pointed at the global reactions $C_{(s)} + 2NiO \rightarrow CO_2 + 2Ni$, $C_{(s)} + NiO \rightarrow CO + Ni$ followed by $CO + NiO \rightarrow CO_2 + Ni$ as the potential reasons for both NiO reduction and carbon removal. This would be explained by the fact that most carbon is produced in stage one, therefore on a reactor bed dominated by NiO rather than Ni. C_(s) and NiO would therefore be in close proximity. When comparing the molar amounts of NiO and C_(s) removed during the N₂ feed shown in Table 5, ratios between 1.6 and 1.8 were calculated (last column of Table 5), which support the above NiO reduction reactions.

[Table 5 here](#)

4. Conclusions

The most suitable sorbents were dolomite, calcite and a high surface area CaCO₃. Adsorption cycling of these sorbents for the prepared CaCO₃ indicated an initial drop in CO₂ intake, while dolomite and calcite remained more stable. The prepared high surface area CaCO₃ exhibited an adsorption capacity similar to dolomite after continual cycling. Lowering the partial pressure of CO₂ also lowered the temperatures at which calcination started upon heating. The partial pressure of CO₂ had an effect on the experimental CO₂ intake, but further experiments are required to study around the likely concentration of 10% CO₂ of the USR process, as well as the effects of repeated cycling and presence of water (varying from 20% to 90% through the three stages of the USR fuel-steam feed), these USR conditions are expected to have detrimental effects of the CO₂ intake according to the recent literature on other CO₂ sorbents.

Very encouraging reformat compositions (>90% dry H₂) were obtained in the initial cycles of USR of methane in the presence of calcined dolomite using a steam to carbon ratio of 4 at a reactor temperature of 650 °C.

The USR process which involves two alternated feeds of air and of methane-steam mixture on a Ni-based OTM reactor bed (without CO₂ sorbent) was shown to operate in two stages during the methane-steam feed. Firstly, the Ni-OTM under its initial oxidised form underwent reduction both by methane and by hydrogen produced from the thermal decomposition of methane. Short-lived carbon formation occurred in the absence of steam reforming, making the steam feed an unnecessary cost. In the experiments presented here, there was a dead time with no hydrogen evolution from the reactor as it was entirely consumed to reduce the NiO

bed. In a second stage, steam reforming initiated, likely the result of sufficient reduced Ni being produced, and the desired hydrogen rich reformat evolved, reaching a dry H₂ content of ca. 74% vol., a high value due to some methane thermal decomposition. Reactor temperatures below 700°C had poor fuel and steam conversion but the lowest CO/CO₂ ratio, which meant a good potential for CO₂ sorption, and shortest dead time. Above 700°C, the dead time was longer. Given the reliance of the steam reforming reaction on reduced Ni catalyst to initiate, two ways of tackling dead-time were considered: one that does not require process modification (increasing methane feed rate), and one that does, in the form of an intermediate fuel-only feed sandwiched between the air feed and the fuel-steam feed. Closure of the carbon and Ni/NiO balances over the full cycle was demonstrated, highlighting the possibility of additional reactions where the carbon deposited during the initial stage of fuel feed reacts with NiO generating CO₂ and CO. Future work will include investigating the USR process in the presence of the CO₂ sorbent identified as best materials, investigating the autothermal behaviour, and testing the suitability of alternative fuels such as pyrolytic biomass and waste tyre oils.

Acknowledgements

The work presented here is financially supported by the Engineering and Physical Science Research Council (EPSRC) under GR/R50677. The authors are also grateful to Dr Phil Ingram at Johnson Matthey for the supply of OTM materials. Masters students A. Hengstenberg-Giron, O. Ahmad, S. Grimwood, and Mark Knowles are also thanked for experimental assistance.

References

- Adanez, J., Garcia-Labiano, F., De Diego, L. F., Fierro, V., 1998. H₂S removal in Entrained Flow Reactors by Injection of Ca-Based Sorbents at High Temperatures. *Energy & Fuels*, 12, 726-733.
- Agnew J., Hampartsoumian E., Jones J.M., Nimmo W., 2000. The simultaneous calcinations and sintering of calcium based sorbents under a combustion atmosphere. *Fuel*; 79, 12, 1515-1523, 2000.

- Chrissafis, K., Dagounaki, C., Paraskevopoulos, K. M., 2005. The effects of procedural variables on the maximum capture efficiency of CO₂ using a carbonation/calcination cycle of carbonate rocks. *Thermochimica Acta*, 428, 193-198.
- Couttenye, R. A., Hoz De Vila, M., Suib, S.L., 2005. Decomposition of methane with an autocatalytically reduced nickel catalyst. *Journal of Catalysis*, 233, 317-326
- Dupont, V., Ross, A. B., Hanley, I., and Twigg, M. V., 2007. Unmixed steam reforming of methane and sunflower oil: a single reactor process for H₂-rich gas. *International Journal of Hydrogen Energy*, 32, 67-79.
- Ishida, M., Zheng, D., Akehata, T., 1987. Evaluation of a Chemical-Looping Combustion Power-Generation System by Graphic Exergy Analysis. *Energy*, 12, 2, 147-154.
- Kumar R. V., Cole J. A., Lyon R. K., 1999. Unmixed Reforming: An Advanced Steam Reforming process. Fuel Division. Preprints of Symposia, 218th ACS National Meeting, August 22-26, New Orleans, LA, 44 (4) 894-898.
- Kumar, R., Moorefield, C., Kulkarni, P., Eiteneer, B., Reinker, J., Zamansky, V and Manning, M. Autothermal Cyclic Reforming and H₂ refueling system. DOE project review May 2004, Philadelphia.
- Lin, S., Harada, M., Suzuki, Y., Hatano, H. Proc. "11th ICCS" San Francisco, 2001
- Lyon R. K., Cole J. A., 2000. Unmixed combustion: an alternative to fire. *Combustion and Flame*; 121, 249-261.
- Marquardt-Mollenstedt, T., Sichler, P, Specht, M., Michel, M., Berger, R., Hein, K. R. G., Hoftberger, E., Rauch, R., Hofbauer, H., New Approach for Biomass Gasification to Hydrogen. 2nd World Conference on Biomass for Energy, Industry and Climate Protection, 10-14 May 2004, Rome, Italy.
- Muradov, N., Smith, F., T-Raissi, A., 2005. Catalytic activity of carbons for methane decomposition reaction. *Catalysis Today*, 2005, 102-103, 225-233.
- Ochoa-Fernandez, E. 2007. Thesis at NTNU, Trondheim, Norway. Chapter 4 paper 6: Effects of steam addition on the properties of high temperature CO₂ ceramic acceptors.
- Reijers, H, Th. J., Valster-Schiermeier, S. E. A., Cobden, P. D, and van den Brink, R. W., 2006. Hydrotalcite as CO₂ sorbent for sorption-enhanced steam reforming of methane. *Industrial Engineering Chemistry Research*, 45, 2522-2530

Richter, H. J., and Knoche, K. F. Reversibility of Combustion Process, ACS Symposium Series, American Chemical Society: Washington, DC, 1983, pp 71-85.

Rizeq, G., West, J., Frydman, A., Subia, R., Zamansky, V., Loreth, H., Stonawski, L., Wiltowski, T., Hippo, E. and Lalvani, S. Fuel-Flexible gasification-combustion technology for production of H₂ and sequestration-ready CO₂. DOE Award N. DE-FC26-00FT40974 Quaterly Technical Progress Report N. 9, January 2003. Reporting period Oct 1, 2002-Dec 31, 2002..

Ross, A. B., Dupont, V., Hanley, I., Ahmad, O. S., Jones, J. M., Twigg, M. V.. Hydrogen Production from Vegetable Oil by Unmixed Reforming. Proceedings of The Seventh International Conference on Technologies and Combustion for a Clean Environment (Clean Air 2003). 7-10th July 2003, Lisbon, Portugal.

Ross, A.B., Dupont, V., Hanley, I, Jones, J.M., Twigg, M. V., 2004. Production of Hydrogen from Sunflower Oil. Abstracts of papers of the American Chemical Society 228: u676-u676 151-fuel part 1 aug 22 2004

Ross, A.B., Hanley, I., Dupont, V., Jones, J.M., Twigg, M.V., 2006. Demonstration of Unmixed Steam Reforming of Vegetable Oil. Science in thermal and chemical biomass conversion Volume1. pp. 444-459. Ed Tony Bridgewater and D.G.B. Boocock. Publ. Antony Rowe Ltd, Chippenham. ISBN 1-872691-97-8.

Son, S.R.and Kim, S.D., 2006. Chemical-Looping Combustion with NiO and Fe₂O₃ in a Thermobalance and Circulating Fluidized Bed Reactor with Double Loops. Industrial Engineering Chemistry Research, 45, 2689-2696.

Zamansky, V., 2002. Unmixed fuel processing for coal. Clean Coal Day in Japan, Tokyo, Sept 3-4, 2002.

Table Legends

Table 1 Theoretical and experimental CO₂ adsorptions of materials tested. Precalcination at 800°C under N₂ flow, then carbonation at 700 °C in pure CO₂ flow. The exp. CO₂ is calculated from CO₂ evolving during second calcination by heating to 800 °C in N₂ flow.

Table 2 Measured times for species breakthrough (t_{0+}) and time from breakthrough to reaching 90% of calibration value ($t_{90} - t_{0+}$) measured by online analysers with and without the silica gel trap present when feeding calibration gas by-passing the reactor.

Table 3 Values of t_{0+} and $t_{90} - t_{0+}$ when feeding calibration gas into the reactor bed at 400°C filled with reduced Ni-OTM, with oxidised NiO-OTM, in the presence and in absence of steam. Above 400°C, reactions of the calibration gases occur but response times are reduced.

Table 4 Process outputs of 'stage 2' of the fuel feed for the OTM containing 27.5 wt % Ni. Flow conditions are 358 sccm of CH₄, 600 sccm of N₂, 0.52 ml min of H₂O (steam to carbon ratio 1.8), 80 g of OTM, total duration 600 s.

Table 5 Ni/NiO-OTM conversions and carbon formation/removal integrated over each feed, forming a balance over a cycle (CH₄/N₂/steam, N₂, air). NiO is reduced during the fuel feed and the N₂ feed, Ni is oxidised during the air feed. Carbon is formed during the fuel feed, but oxidised during the N₂ and air feeds. Last column shows the ratio of NiO reduced to C oxidised to CO₂ during N₂ feed.

Table 1

Sorbent	Formula	Wt % Ca	Wt % Mg	Theo. CO ₂ (g/kg sorb)	Exp. CO ₂ (g/kg sorb)	capacity used (%)
Spanish dolomite (Sierra de Arcos)	CaMg(CO ₃) ₂ , SiO ₂ , Al ₂ O ₃ , Fe ₂ O ₃	21.0	11.6	237.0*	151.6	64.0
Calcite	CaCO ₃	40.0	-	439.7	197.1	44.8
Magnesite	MgCO ₃	-	28.8	521.9	20.2	3.9
Limestone	CaCO ₃	40.0	-	439.7	127.0	28.9
CaCO ₃ from acetate	CaCO ₃	40.0	-	439.7	199.9	45.5
CaCO ₃ on γ -Al ₂ O ₃		10	-	109.8	30.4	27.7
Mg-hydrotalcite	Mg _{0.75} Al _{0.25} (OH) ₂(CO ₃) _{0.125} .0.5H ₂ O	-	24.1	72.8	13.7	18.8
Ca-hydrotalcite	Ca _{0.75} Al _{0.25} (OH) ₂(CO ₃) _{0.125} .0.5H ₂ O	34.4	-	63	15.9	25.2
Blank γ alumina	γ -Al ₂ O ₃	-	-		88.6	

* MgO does not re-carbonate in calcined dolomite

Table 2

Conditions	t_{0+} H ₂	t_{0+} CH ₄	t_{0+} CO ₂	t_{0+} CO	$t_{90} - t_{0+}$ H ₂	$t_{90} - t_{0+}$ CH ₄	$t_{90} - t_{0+}$ CO ₂	$t_{90} - t_{0+}$ CO
By-pass reactor								
With silica gel	20	15	15	15	17	15	20	13
Without silica gel	20	15	15	20	19	10	10	6

Table 3

Conditions @400 °C, calib. gas	t_{0+} H ₂	t_{0+} CH ₄	t_{0+} CO ₂	t_{0+} CO	$t_{90} - t_{0+}$ H ₂	$t_{90} - t_{0+}$ CH ₄	$t_{90} - t_{0+}$ CO ₂	$t_{90} - t_{0+}$ CO
no steam, oxidised bed	40	35	60	65	55	50	110	55
steam oxidised bed	40	35	55	55	72	80	79	55
no steam reduced bed	45	40	70	70	132	72	125	85
steam reduced bed	40	40	65	50	93	65	85	50

Table 4

T (°C)	Dead Time (s)	% conv CH ₄	% conv H ₂ O	% sel CO ₂	% sel CO	% sel C _(s)	% dry (0N ₂) H ₂	H ₂ Prod Eff	CO/CO ₂
600	30	49.7	40.7	57.1	42.4	0.9	63.5	45.5	0.74
600	40	54.5	42.4	54.5	43.4	1.8	65.2	48.8	0.80
650	90	74.7	47.9	38.3	58.8	3.3	70.8	62.0	1.54
650	65	78	50.4	40.2	57	2.8	71.6	64.6	1.42
700	85	88.5	52.4	33.4	63.9	3.2	73.5	71	1.91
700	80	90.3	52.5	31.2	65.1	3.6	74	72.4	2.09
750	90	96.5	52.2	27.2	68.9	3.9	74.8	75.1	2.53
750	80	97.2	51	26.5	68.5	5.1	75.1	75.2	2.58
800	100	98.9	48.7	24	70.3	5.7	75.3	75.1	2.93
800	80	99.1	47.3	23.6	70.1	6.3	75.2	74.3	2.97

Table 5

T (°C)	% conv fuel feed	% conv N ₂ feed	% conv fuel + N ₂ feeds	% conv Air feed	Mol ×10 ³ fuel feed	Mol×10 ³ N ₂ +Air feeds	Mol×10 ³ N ₂ feed	Mol×10 ³ Air feed	NiOconv/C(S) oxid. during N ₂ feed
	NiO→Ni	NiO→Ni	NiO→Ni	Ni→NiO	C _(s) prod	C _(s) oxid	C _(s) oxid	C _(s) oxid	
600	6.0	1.6	7.6	6.1	6	4.23	3.3	0.93	1.8
600	6.5	1.9	8.4	8.8	4.7	4.62	4.0	0.62	1.8
650	9.1	2.4	11.5	19.6	7.1	6.9	5.4	1.5	1.7
650	10.1	2.2	12.3	12.7	6.6	5.6	4.9	0.7	1.7
700	14.4	2.6	17.0	18.2	11	6.55	5.8	0.75	1.7
700	15.6	2.7	18.3	17.7	8.1	7.4	6.3	1.1	1.6
750	21.4	2.5	23.9	26.2	12	7.9	5.8	2.1	1.6
750	21.6	3.2	24.8	25.8	11	9.6	7.1	2.5	1.7
800	30.3	3.0	33.3	33.1	14	12.8	6.9	5.9	1.6
800	28.0	3.3	31.3	31.9	11	12.7	7.4	5.3	1.7

Figures

Fig. 1. Illustration of unmixed reforming reactor operation. Dark regions are hotter from exothermic reactions (air feed) or heat storage (fuel feed). Although not part of the ideal process, carbon formation under fuel feed and oxidation under air is observed in the experiments.

Fig. 2. Diagram of apparatus used for OTM and sorbent testing. Legend:

1. Temperature controller, 2. Ni/Cr heating coil, 3. Quartz silica reactor, 4. K type thermocouple, 5. Temperature data logger, 6. Bypass line, 7. Water trap, 8. OTM resting on sinter, 9. On-line analysers (ABB Caldos, Uras and Magnos)

Fig. 3 Diagram of the bench scale unmixed steam reforming process using a methane feed in the fixed bed reactor.

Fig. 4 Carbonation capacity/regeneration capacity over repeated cycles for dolomite, calcite and CaCO_3 from calcium acetate.

Fig. 5 Mass vs. temperature for Spanish dolomite in TGA experiments of cycled calcinations (heating) and carbonation (cooling). Particles size 1-2 mm, heating and cooling rates $10^\circ\text{C}/\text{min}$, comparison between flow of pure CO_2 , pure N_2 and 50% CO_2 /50% N_2 . Downward arrows indicate the run is under heating conditions, upward arrows indicate cooling.

Fig. 6 Dry H_2 (left y axis), and dry CH_4 , CO_2 and CO concentrations on vol % basis. Conditions were 650°C , S:C ratio of 4, 20 g of dolomite, 60 g of OTM. (800 sccm CH_4 , no N_2 diluent)

Fig. 7 Dry gas concentration on a volume percent basis for H_2 , CH_4 , CO_2 and CO for conversion at 750°C , steam to carbon ratio of 1:8, 80g of OTM, no CO_2 sorbent, flow conditions 358 sccm of CH_4 in 600 sccm of N_2 diluent.

Fig. 8 Conversion histories of methane, steam, and OTM reduction for the mid reactor temperature for conditions as in Fig.7.

Fig. 9 Selectivity to $\text{C}_{(\text{s})}$, CO and CO_2 for conditions as in Fig. 7.

Fig. 10 Dry H_2 mol % corrected for zero nitrogen content, OTM reduction rate and carbon formation rate, for conditions as in Fig.7.

Fig. 11 Reactor temperature histories under during the air feed. This feed followed the fuel-steam feed at 750 °C. Flow of air was 2000 sccm (equivalent to 3.125×10^{-4} mol s⁻¹ of O₂).

Thermocouple locations: top, mid-reactor and bottom.

Fig. 12 Conversions of oxygen and of OTM under air flow, OTM oxidation rate under air feed, conditions as in Fig.11.

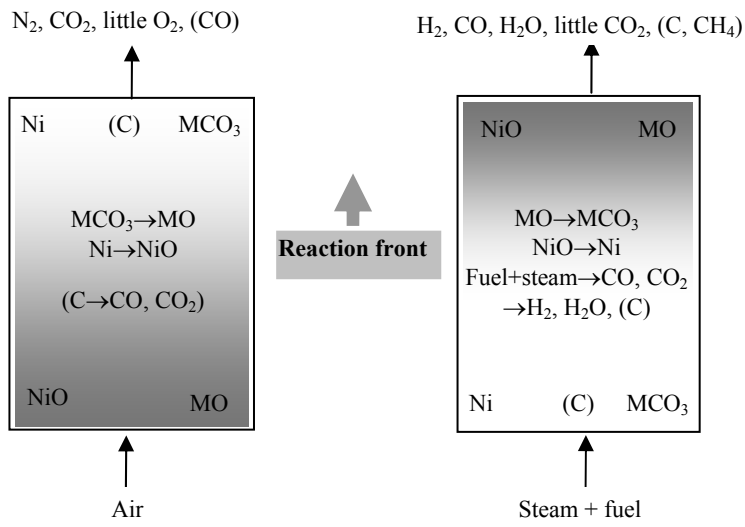


Figure 1

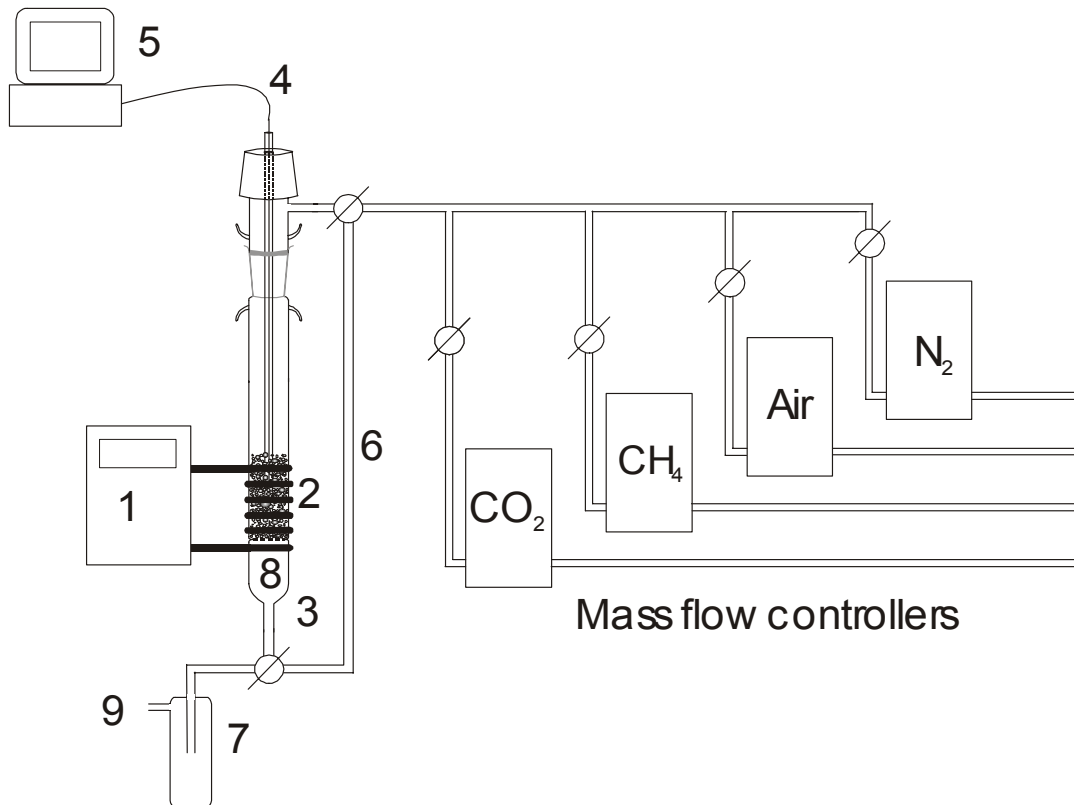


Figure 2

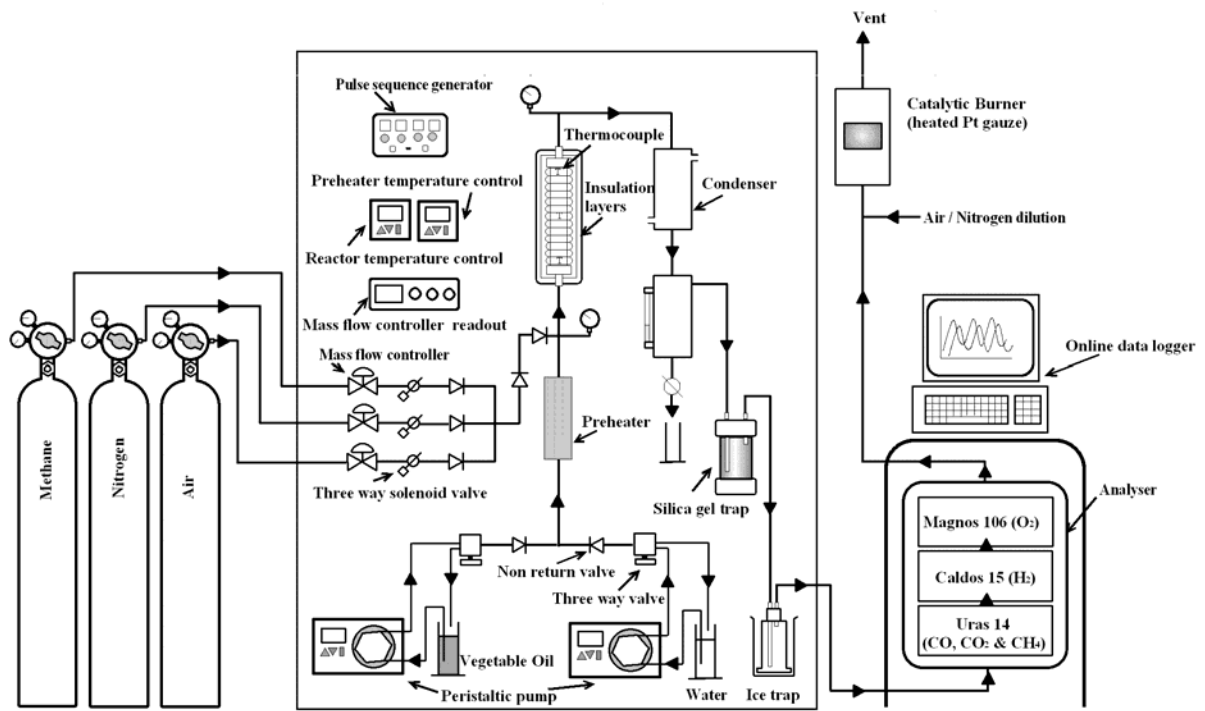


Figure 3

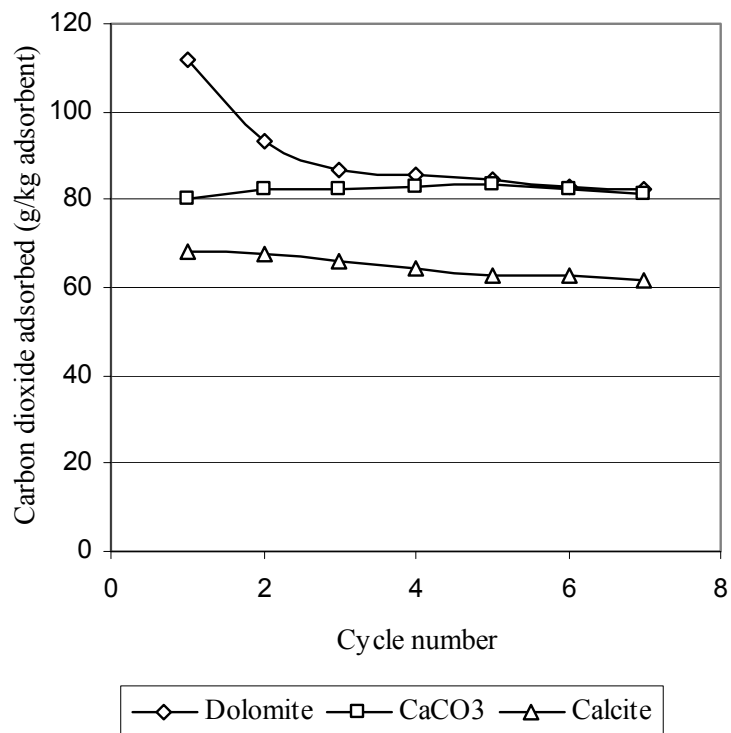


Figure 4

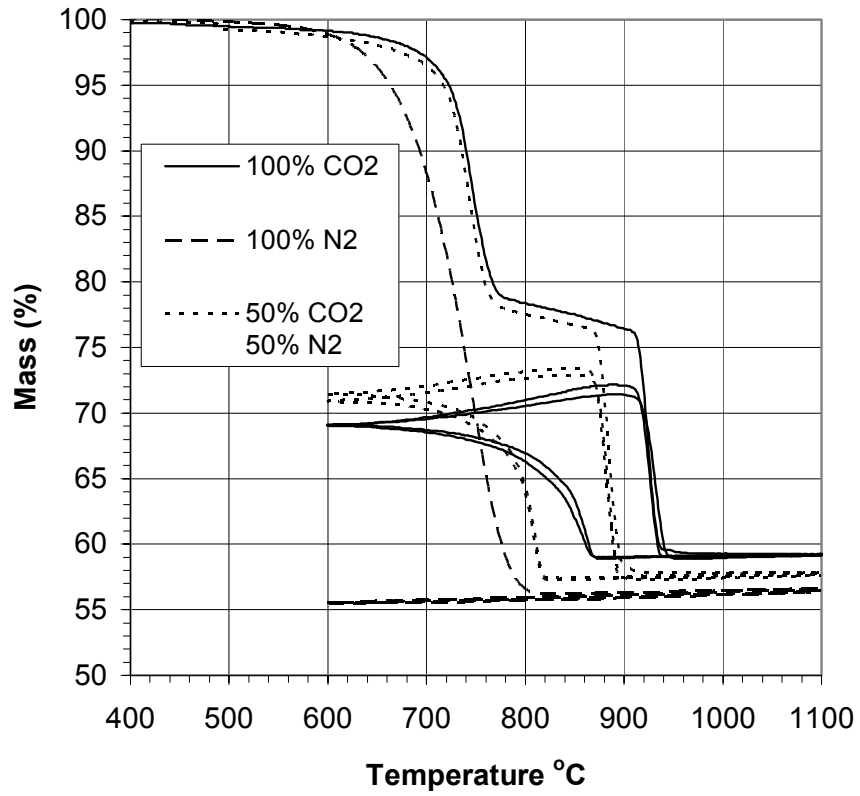


Figure 5

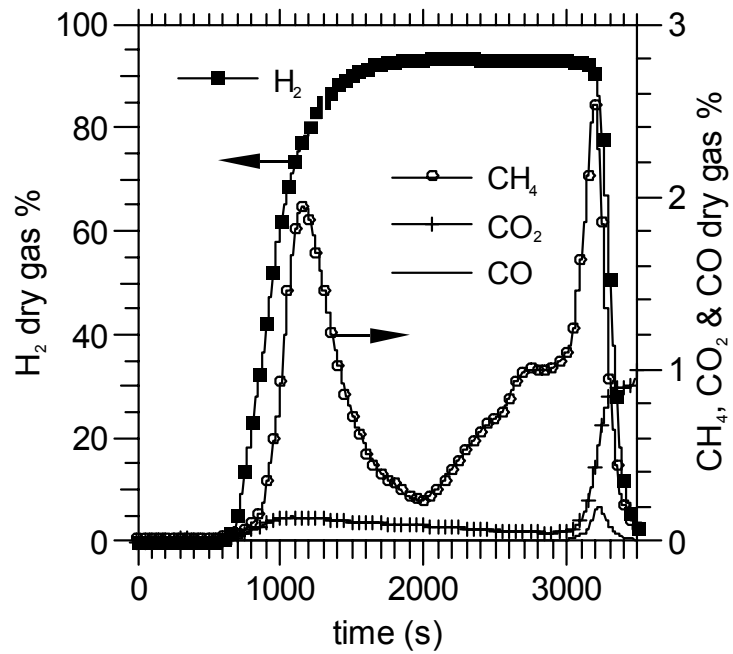


Figure 6

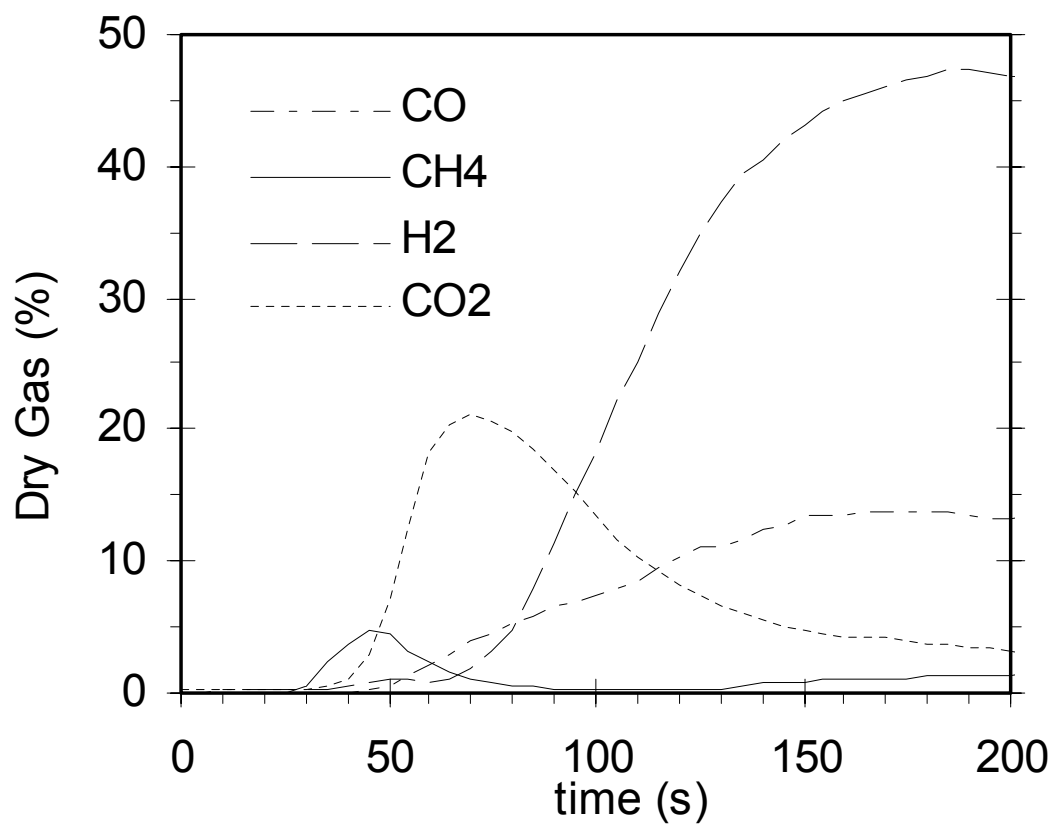


Figure 7

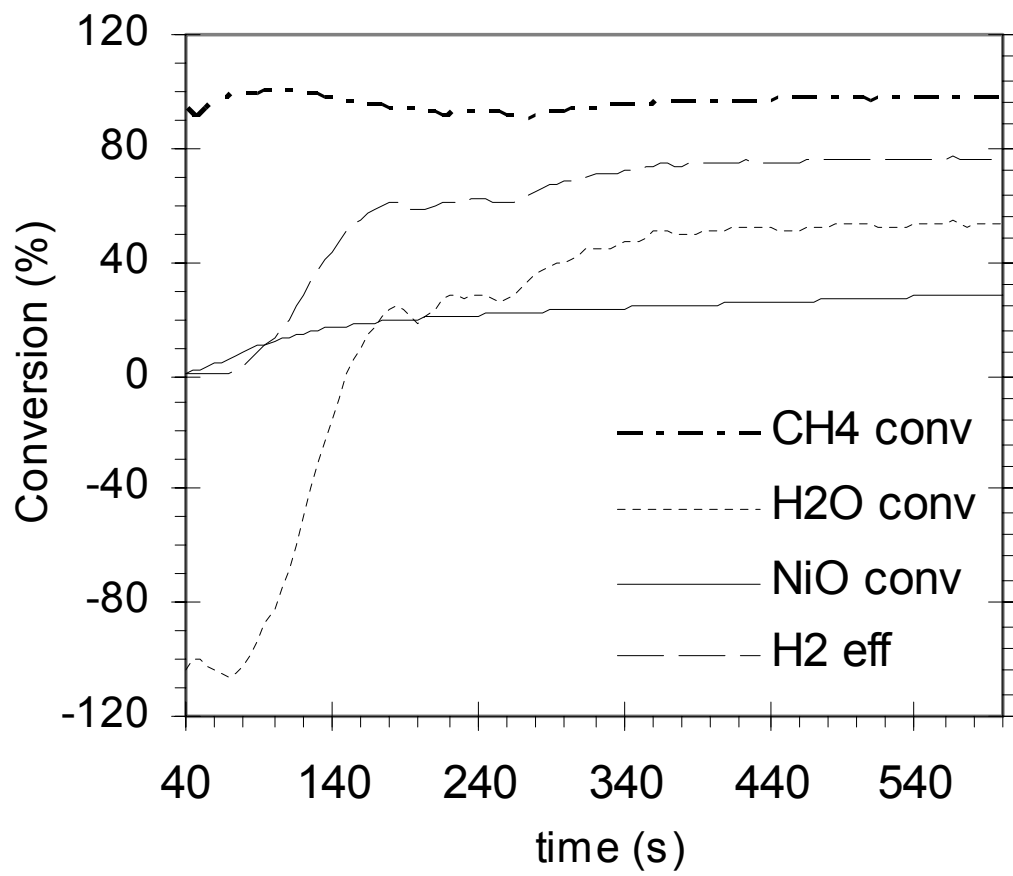


Figure 8

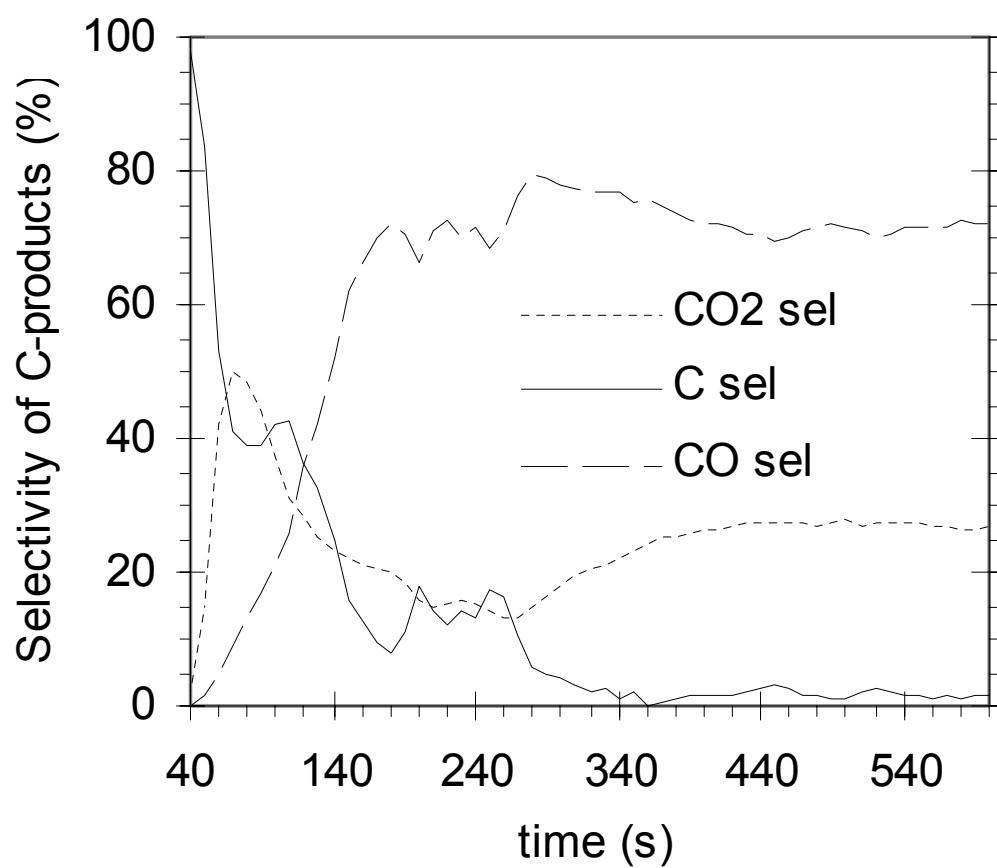


Figure 9

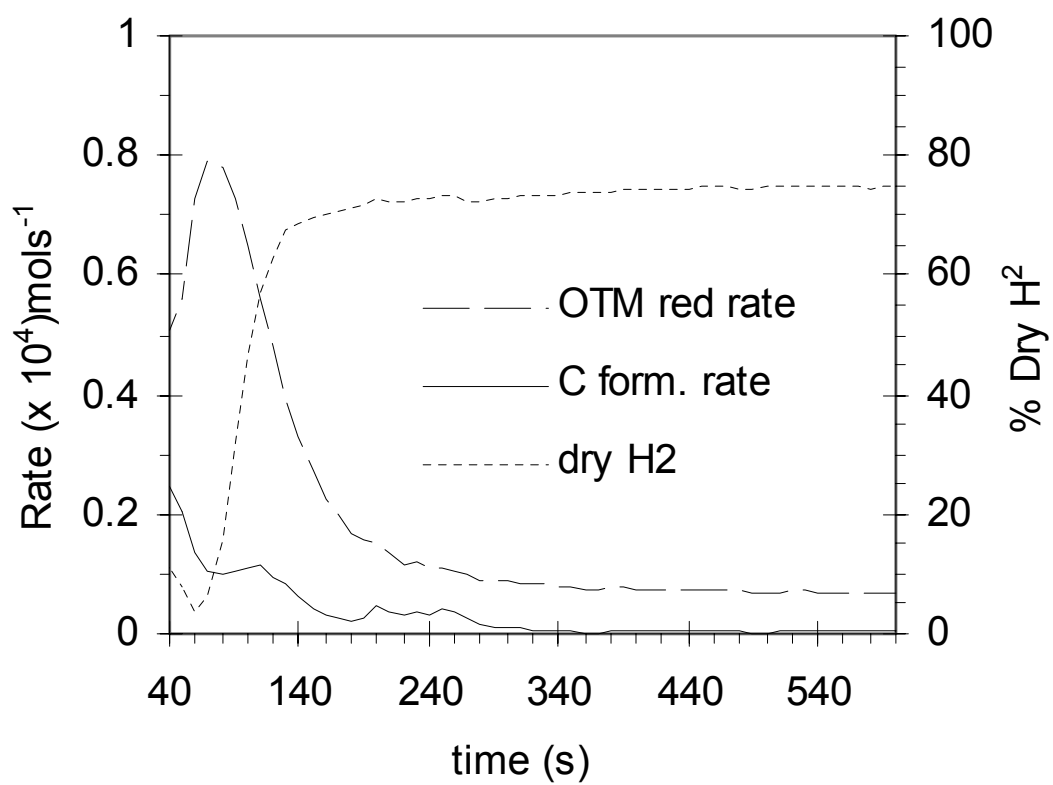


Figure 10

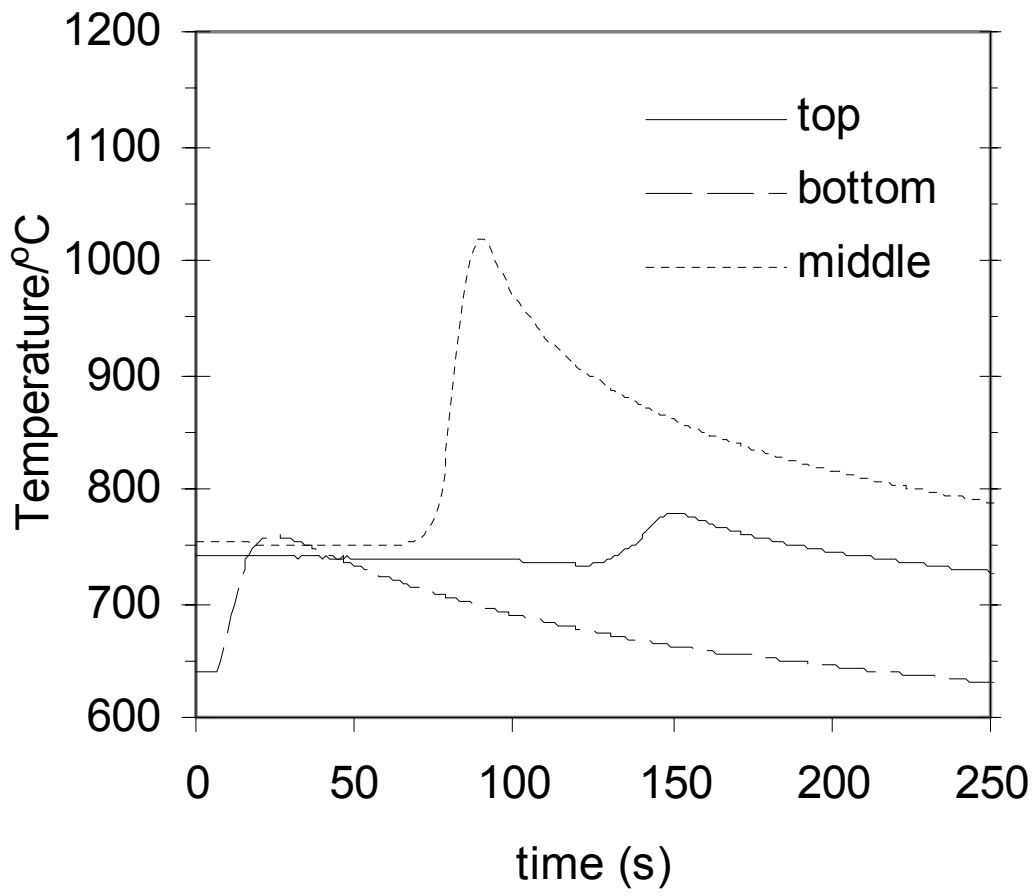


Figure 11

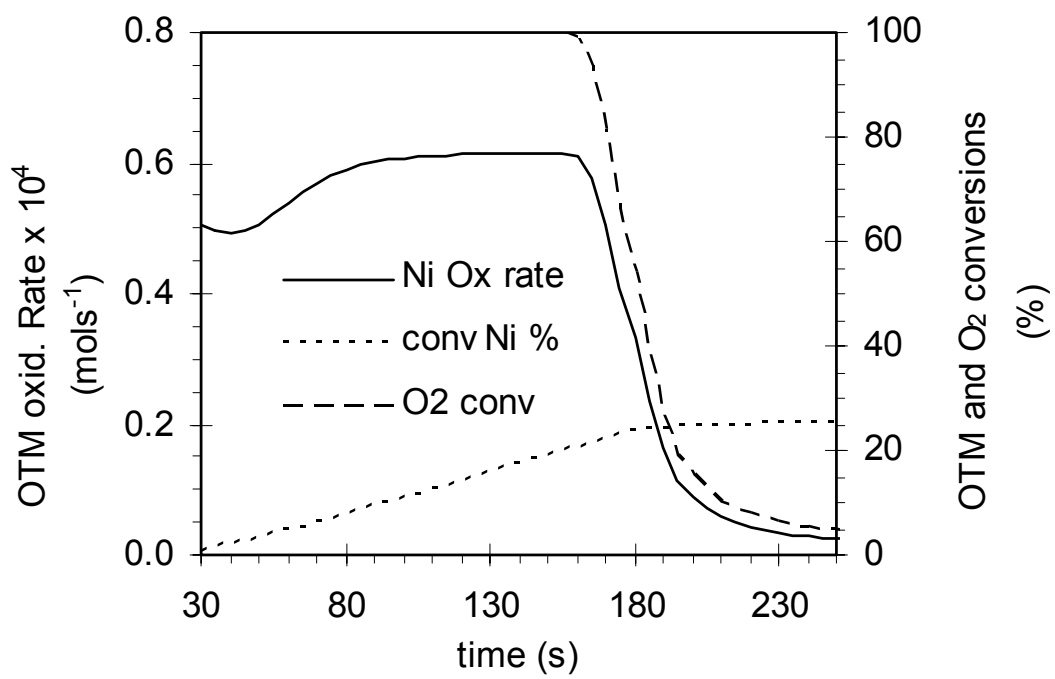


Figure 12